Stabilized Gauged Formulation of Darwin Model for FEM Computation of Industrial Applications

Houssein Taha, Zuqi Tang, Thomas Henneron, Yvonnick Le Menach, Jean-Pierre Ducreux, Florentin Salomez

Stabilized Gauged Formulation of Darwin Model for FEM Computation of Industrial Applications

Houssein Taha[1], Zuqi Tang[1], Thomas Henneron[1], Yvonnick Le Menach[1], Jean-Pierre Ducreux[2], Florentin Salomez[1]
[1]Univ. Lille, Arts et Metiers Institute of Technology, Centrale Lille, Junia, ULR2697-L2EP, F-59000 Lille, France
[2]EDF R&D, ERMES, 7 Boulevard Gaspard Monge, 91120 Palaiseau, France

The Darwin model attracts more and more attention in the research area recently, which simultaneously incorporates resistive, capacitive, and inductive effects but neglecting the radiation one. For our industrial application needs, the finite element (FE) system to solve derived from the Darwin model generally has a large size, which is out of the support of the direct solvers due to the memory limitation. In this work, a specially designed formulation adopted with iterative solvers is proposed for industrial applications. Moreover, a detailed comparison of different cases is carried on two different examples.

***Index Terms*—Darwin model, edge element, finite element analysis, linear solver**

I. Introduction

The recent development towards the system with higher integration of increasing power and information densities brings up systems operating at the frequency in the middle range, where the resistive, capacitive, and inductive effects should be considered simultaneously. The modeling of the capacitive phenomena including the inductive effects becomes critical, especially in the case of a power converter with high switching frequencies supplying an electrical device. In this context, the Darwin model attracts more and more attention recently in the research area [1]–[5]. In the literature, the mixed vector/scalar potential $\mathbf{A}/\varphi$ formulation of Darwin model without gauge conditions is presented in [2], where the iterative solvers as BiCGSTAB or the GMRES are applied for the resulting non-symmetric and singular system. In case of a large difference in the value of the material coefficients, the ill-conditioning might decrease the performance of the iterative solver significantly. To address the instability and the non-symmetric issues, in our previous work, a stabilized Coulomb gauged $\mathbf{A}/\varphi$ formulation is proposed in [4]. The Coulomb-type gauge has been additionally imposed as a third equation by a Lagrange multiplier, which ensures the symmetry of the matrix without any additional regularization. However, the proposed formulation requires the use of direct solvers since the resulting finite element (FE) system corresponds to a saddle point problem, where the iterative solver is not preferable.

At the point of view of industrial applications, it is still a challenge to use the above formulation directly. Due to the complex geometries considered in industrial problems, as well as its operating frequency, the FE system to solve usually has huge degrees of freedom (DoFs), which is out of the support of the direct solver, even it is known that the advanced direct solver can handle a system until 30 million DoFs nowadays. Alternatively, the iterative solver is still a good choice because it can solve a huge system beyond the limitation of direct solvers. Due to the ill-conditioning, an adapted preconditioner should be developed. However, to the best of the authors' knowledge, a stable preconditioner is still an open problem in the research area for the Darwin model.

To address this numerical issue arising in industrial applications of the Darwin model, a specially designed formulation adopted with iterative solvers is proposed in this work. Inspired by the use of double Lagrange multipliers [6], the proposed formulation can be successfully applied to handle the huge matrix system derived from the complex industrial applications. Besides, a detailed comparison of the performance of the above-mentioned formulations with different solvers is carried out on two different examples.

The paper is organized as follows: all the considered formulations are recalled and presented in Section II. In Section III, by considering two different examples, the comparison between different cases is given. Finally, our conclusion is given in Section IV.

II. Numerical models

In the following, the three above-mentioned formulations, denoted F1, F2, and F3, respectively, will be presented in the frequency domain.

A. F1 Formulation

The classical $\mathbf{A}/\varphi$ formulation of Darwin model without entering the gauge conditions given in [2] reads

$$\begin{aligned} \mathbf{rot}\,(\nu\mathbf{rot}\,\mathbf{A}) + \sigma(j\omega\mathbf{A} + \nabla\varphi) + j\omega\varepsilon\nabla\varphi = \mathbf{0}, \\ \nabla\cdot(-\sigma(j\omega\mathbf{A} + \nabla\varphi) - j\omega\varepsilon\nabla\varphi) = 0 \end{aligned} \tag{1}$$

where ν is the magnetic reluctivity (the inverse of the magnetic permeability μ), σ and ε are the electric conductivity and permittivity, respectively.

As no gauge is applied, the system (1) does not have the uniqueness of the solution for the magnetic vector potential $\mathbf{A}$, which means the system is singular. However, the physical quantities (such as the magnetic flux density $\mathbf{B}$ and the electric field $\mathbf{E}$) are unique. To ensure the uniqueness of the potential $\mathbf{A}$, both the implicitly imposed Coulomb-type gauge by the iterative solver [7] or/and by the direct solver [8], and the tree gauge [9] will be applied in the following numerical part.

B. F2 Formulation

By introducing a Lagrange multiplier p and rewriting the current continuity equation using the Coulomb gauge condition, the resulting matrix becomes symmetric as reported in [4]. Then, the stabilized Coulomb gauged $\mathbf{A}/\varphi$ formulation reads

$$\begin{aligned} \textbf{rot}\,(\nu\textbf{rot}\,\mathbf{A}) + \sigma(j\omega\mathbf{A} + \nabla\varphi) + j\omega\varepsilon\nabla\varphi - j\omega\varepsilon\nabla p &= \mathbf{0}, \\ \nabla\cdot(-\sigma(j\omega\mathbf{A} + \nabla\varphi) - j\omega\varepsilon\nabla\varphi) - j\omega\nabla\cdot(\varepsilon\mathbf{A}) &= 0, \\ j\omega\nabla\cdot(\varepsilon\mathbf{A}) &= 0. \end{aligned} \tag{2}$$

It can be found that the resulting system is symmetric but is a saddle point problem where ad-hoc solvers and preconditioners are needed [10]. The direct solver can provide an accurate solution in this case.

C. F3 Formulation

Inspired by our previous work [6], to avoid solving the saddle point problem, based on the F2 formulation, the double Lagrange multiplier method is applied here, which consists in duplicating the scalar p into two scalar unknowns denoted p_1 and p_2 with $p_1 = p_2$. By rewriting the F2 formulation, our proposed formulation reads

$$\begin{aligned} \textbf{rot}\,(\nu\textbf{rot}\,\mathbf{A}) + \sigma(j\omega\mathbf{A} + \nabla\varphi) + j\omega\varepsilon\nabla\varphi \\ -j\omega\varepsilon\nabla p_1 - j\omega\varepsilon\nabla p_2 &= \mathbf{0}, \\ \nabla\cdot(-\sigma(j\omega\mathbf{A} + \nabla\varphi) - j\omega\varepsilon\nabla\varphi) - j\omega\nabla\cdot(\varepsilon\mathbf{A}) &= 0, \\ j\omega\nabla\cdot(\varepsilon\mathbf{A}) + p_1 - p_2 &= 0, \\ j\omega\nabla\cdot(\varepsilon\mathbf{A}) + p_2 - p_1 &= 0. \end{aligned} \tag{3}$$

It can be seen that the resulting FE system is also symmetric and gauged.

Regarding the DoFs for all three formulations, F2 has an additional nodal unknown p in comparison with F1, which introduces normally $1/6$ DoFs, while F3 has two additional nodal unknowns, namely p_1 and p_2. It should be mentioned here, the proposed formulation is not an "optimal" one in theory, but rather a possibly good one that can break the bottleneck we meet in industrial applications.

III. Numerical Results

In this part, the performance of three formulations will be illustrated under different cases for two different examples.

For the computational configurations, as summarized in Table I, MUMPS is used as the direct solver to solve the linear system derived from F1 and F2 formulations while BiCGSTAB is used as the iterative solver for both F1 and F3 formulations, with a classical Split-Jacobi preconditioner. Furthermore, as the F1 formulation is not gauged, the tree gauge and the implicitly imposed Coulomb gauge are considered for both direct and iterative solvers.

TABLE I
Different cases for the studied formulations.

Formulations	Solving Methods	
	BiCGSTAB	MUMPS
F1	✓	✓
F2	-	✓
F3	✓	-

Two different numerical examples are considered here: a first academic one with analytical solution [3] and a second industrial one with measurement [11]. All the above formulations have been implemented in our software *code_Carmel*[1] to provide the numerical simulation results.

A. Parallel-Plate Capacitor

Firstly, we consider an academic example as given in Fig. 1(a), which is well studied for the Darwin model. A sinusoidal voltage excitation with a magnitude $V_\mathrm{s} = 1$ V is applied at the plate terminals. The frequency interval to investigate is $[1 : 10^9]$ Hz. The electric conductivity of the conductor is taken as 50 kS/m. For the relative permittivity, it is set as 1 for the conductor (grey part) and 10 for the dielectric (green part), while the relative permeability is set as 10^3 and 1, respectively. The used mesh features 100,626 elements including 17,073 nodes and 118,141 edges, as shown in Fig. 1(b).

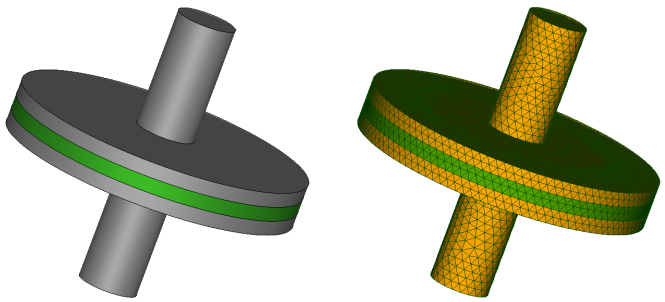

(a) Geometry (b) Mesh

Fig. 1. Geometry and considered mesh of the parallel-plate capacitor.

1) Global results

The magnitude of the current flowing out of the terminal of the capacitor as a function of the frequency is plotted in Fig. 2, for all the cases with F1, F2, and F3 formulations. As reported in [3], the current is proportional to the input voltage frequency. Indeed, the current increases linearly as a function of the frequency (black curve). The results obtained by different cases are very close in the interval $[1 : 10^7]$ Hz, showing the stability of all the formulations/solvers in this interval. However, from 10 MHz, the difference between different solutions can be observed as shown in the zoom part of Fig. 2.

[1] https://code-carmel.univ-lille.fr/

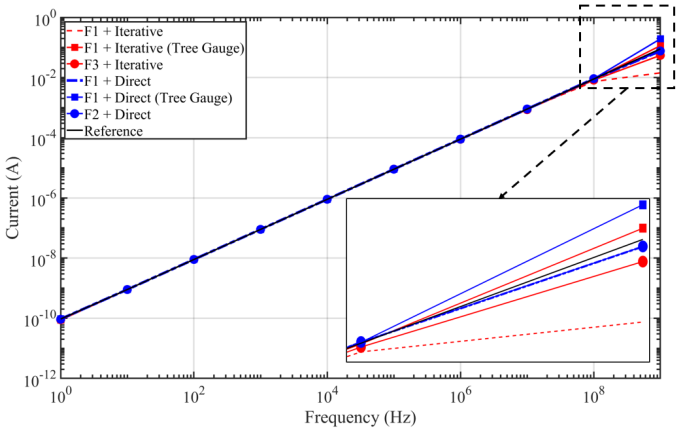

Fig. 2. Magnitude of currents with respect to frequencies using BiCGSTAB iterative solver (in red) and MUMPS direct solver (in blue) in $[1 : 10^9]$ Hz.

Globally, the accuracy of the solutions with the direct solver (in blue) is better than the one with the iterative solver (in red). With the direct solver, the F1 formulation has exactly the same solution as the F2 formulation. But as F1 is non-symmetric, the computational time is much more, which can be verified in Fig. 3.

Now, regarding the results with the iterative solver, it can be found that our proposed F3 formulation is better than both cases with the F1 formulation. In addition, the F1 formulation with tree gauge provides more precision than the ungauged case (which is totally in contrast with the direct solver). However, the use of tree gauge for the magnetic vector potential $\mathbf{A}$ suffers from the deterioration of the condition number of the matrix [12], as shown in Fig. 3. Despite that the gauged formulations need to take more computational time, they can provide a more accurate solution than ungauged ones.

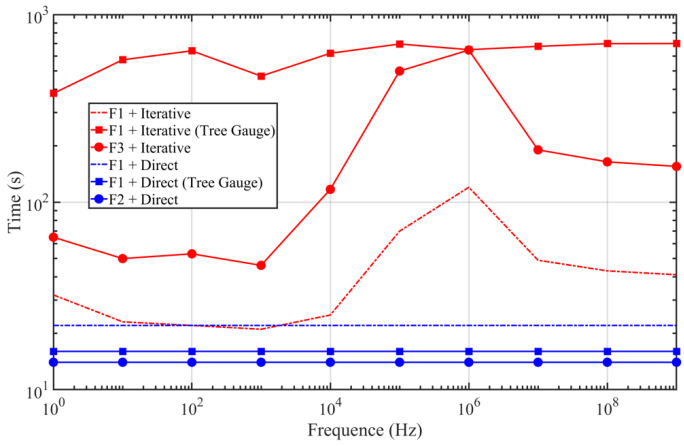

Fig. 3. Computational time for different cases with respect to frequencies.

In the following, to investigate the stability of the F3 formulation on the mesh, five meshes with different global refinement levels are considered. The numerical results are compared with the results obtained by F2. The magnitude of the current flowing out of the terminal of the conductor with different meshes is presented in Table II. It can be observed that, with different meshes, our proposed formulation can get close results with the F2 formulation. Furthermore, it can handle the huge mesh as 30 million DoFs where the direct solver is not available.

TABLE II
THE PERFORMANCE OF DIRECT SOLVER (MUMPS) AND ITERATIVE SOLVER (BICGSTAB) WITH A SPLIT-JACOBI PRECONDITIONER VERSUS THE NUMBER OF ELEMENTS FOR $f = 1$ MHz.

Number of Elements	F2	I_{F2} (A)	F3	I_{F3} (A)
50k	✓	8.966×10^{-5}	✓	8.898×10^{-5}
500k	✓	8.950×10^{-5}	✓	8.938×10^{-5}
2M	✓	8.943×10^{-5}	✓	8.928×10^{-5}
15M	✓	8.939×10^{-5}	✓	8.892×10^{-5}
30M	-	-	✓	8.886×10^{-5}

2) *Local results*

The local results are compared in the following by considering a mesh of 2,607,495 tetrahedrons with 433,986 nodal unknowns and 3,036,297 edge unknowns. As shown in Fig. 4 and Fig. 5, the magnetic and the electric fields simulated with F2 and F3 formulations are compared for $f = 1$ MHz.

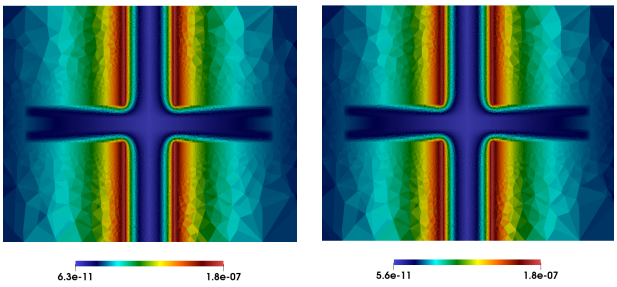

(a) MUMPS (b) BiCGSTAB

Fig. 4. Magnitude of the magnetic field $\mathbf{B}$ for $f = 1$ MHz simulated with both F2 and F3 formulations.

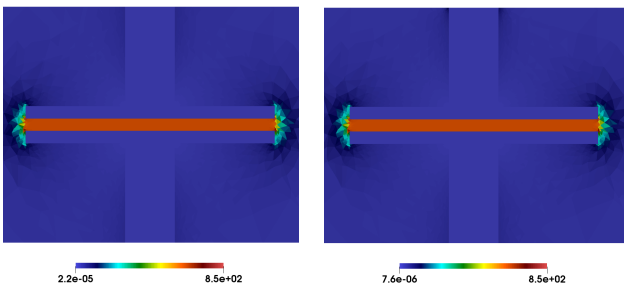

(a) MUMPS (b) BiCGSTAB

Fig. 5. Magnitude of the electric field $\mathbf{E}$ for $f = 1$ MHz simulated with both F2 and F3 formulations.

Due to the skin effect at $f = 1$ MHz, the magnetic field is restricted to a small layer and shows close results with the two cases. Similarly, in both cases, a high field strength with the same amplitude appears in the dielectric region between the two conductors.

B. *Industrial transformer*

Secondly, an industrial case [11] is considered in this part represented by two windings wounds in the same direction

around a toroidal core as shown in Fig. 6. The conductor used for the windings (in gold color) is made of copper, which is insulated by the enamel material. The toroid used for this experiment is of material N30 presented in gray in Fig. 7 where the thickness of the blue part is 0.25 mm. More information about the different materials can be found in [11].

Fig. 6. Toroidal core with two windings.

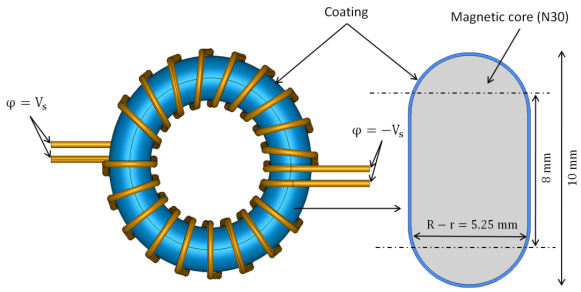

Fig. 7. 3-D model of the transformer.

Two meshes with different refinement levels are considered in this example. On the one hand, since the direct methods suffer from limitations in terms of DoFs, a first mesh with about 8 million elements is used, which features 7,924,176 tetrahedrons including 1,388,382 nodes and 9,315,509 edges. As shown in Fig. 8, two numerical computations are done with F2 and F3 formulations represented in black and green colors, respectively. On the other hand, in order to perfectly handle the skin effect at high frequencies, a second mesh with about 30 million elements, features 29,832,477 tetrahedrons including 5,257,323 nodes and 35,093,396 edges, is considered. The numerical computation is done only with the F3 formulation. The results are represented in red in Fig. 8. The measurement results (in blue) have been provided to validate the simulation results obtained with the Darwin model for three cases.

The modulus of the impedance Z as well as the phase, as a function of the frequency obtained from the Darwin model, are presented in Fig. 8. The modulus of Z obtained with the different cases shows a good agreement in the range of intermediate frequencies, in particular, around the resonant frequency. Besides, with the refined mesh, the F3 formulation shows a closer agreement with the measurements compared to the other cases.

IV. Conclusion

The applications of the Darwin model on the industrial problems introduce huge FE systems to solve. To break the computational limitations linked to the huge DoFs of industrial problems, a specially designed formulation with iterative solvers is proposed. The proposed symmetric Darwin formulation using a Coulomb gauge and double Lagrange multipliers exhibits robust behavior in a wide frequency range. Furthermore, a systematic comparison between different solvers and different formulations is given for two examples.

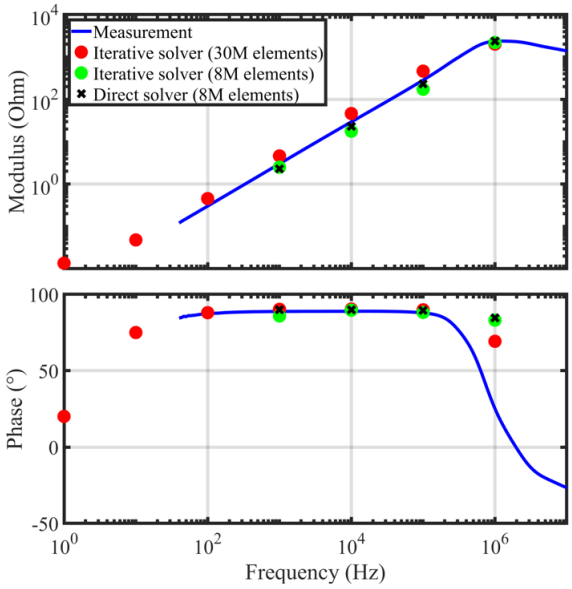

Fig. 8. Modulus of impedance and the phase computed with respect to frequencies.

References

[1] J. Larsson, "Electromagnetics from a quasistatic perspective," *American Journal of Physics*, vol. 75, 07 2006.

[2] S. Koch, H. Schneider, and T. Weiland, "A low-frequency approximation to the Maxwell equations simultaneously considering inductive and capacitive phenomena," *IEEE Transactions on Magnetics*, vol. 48, pp. 511–514, Feb. 2012.

[3] Y. Zhao, "Robust full-wave Maxwell solver in time-domain using magnetic vector potential with edge elements," *IET Science, Measurement & Technology*, vol. 11, pp. 746–752(6), September 2017.

[4] Y. Zhao and Z. Tang, "A novel gauged potential formulation for 3-D electromagnetic field analysis including both inductive and capacitive effects," *IEEE Transactions on Magnetics*, vol. 55, pp. 1–5, June 2019.

[5] M. Clemens, B. Kähne, and S. Schöps, "A Darwin time domain scheme for the simulation of transient quasistatic electromagnetic fields including resistive, capacitive and inductive effects," in *2019 Kleinheubach Conference*, pp. 1–4, 2019.

[6] M. Aubertin, T. Henneron, O. Boiteau, F. Piriou, P. Guerin, and J.-C. Mipo, "Single and double Lagrange multipliers approaches applied to scalar potential formulation in magnetostatic fem," *Przeglad Elektrotechniczny*, vol. 86, pp. 119–122, 01 2010.

[7] Z. Ren, "Influence of the RHS on the convergence behaviour of the curl-curl equation," *IEEE Transactions on Magnetics*, vol. 32, no. 3, pp. 655–658, 1996.

[8] Z. Tang, Y. Zhao, and Z. Ren, "Auto-gauging of vector potential by parallel sparse direct solvers—numerical observations," *IEEE Transactions on Magnetics*, vol. 55, no. 6, pp. 1–5, 2019.

[9] P. Dular, A. Nicolet, A. Genon, and W. Legros, "A discrete sequence associated with mixed finite elements and its gauge condition for vector potentials," *IEEE Transactions on Magnetics*, vol. 31, no. 3, pp. 1356–1359, 1995.

[10] M. Benzi, G. H. Golub, and J. Liesen, "Numerical solution of saddle point problems," *Acta Numerica*, vol. 14, p. 1–137, 2005.

[11] H. Taha, Z. Tang, T. Henneron, Y. Le Menach, F. Salomez, and J.-P. Ducreux, "Numerical simulation-based investigation of the limits of different quasistatic models," *Applied Sciences*, vol. 11, no. 23, 2021.

[12] H. Igarashi, "On the property of the curl-curl matrix in finite element analysis with edge elements," *IEEE Transactions on Magnetics*, vol. 37, no. 5, pp. 3129–3132, 2001.